

Comparative Analysis on the Impact of Electrode Morphologies on Lithium-Ion Battery Performance

A. Lombardo Pontillo¹, A. Querio¹, E. Buccafusco¹, G. Boccardo¹, D. Marchisio¹
1. DISAT, Politecnico di Torino, Turin, Italy.

Abstract

The morphology of electrode materials plays a crucial role in determining the performance of lithium-ion batteries. Traditional computational models often simplify graphite flakes as uniformly sized spheres, which limits their predictive accuracy. In this study, we present a computational workflow that overcomes these limitations by incorporating a more realistic representation of graphite morphologies. This workflow is designed to be flexible and reproducible, enabling efficient evaluation of electrochemical performance across diverse material structures. By exploring different graphite morphologies, our approach accelerates the optimization of material preparation techniques and processing conditions. Our findings reveal that incorporating greater morphological complexity leads to significant deviations from classical model predictions. Instead, our refined model offers a more accurate representation of battery discharge behavior, closely aligning with experimental data. This improvement underscores the importance of detailed morphological descriptions in advancing battery design and performance assessments. To promote accessibility and reproducibility, we provide the developed code for seamless integration with the COMSOL API, allowing researchers to implement and adapt it easily. This computational framework serves as a valuable tool for investigating the impact of graphite morphology on battery performance, bridging the gap between theoretical modeling and experimental validation to enhance lithium-ion battery technology.

Keywords: Lithium-ion batteries; 3D Microscale modeling; COMSOL API; Particles generation.

Introduction

In the design of energy storage systems, mathematical models that efficiently and accurately describe lithium-ion battery (LiB) behavior are essential. Many models use a reduced-order description, such as one-dimensional in the collector–separator direction, assuming uniform behavior in the other dimensions. A well-known example is the Doyle-Fuller-Newman (DFN) model [1], which solves non-linear partial differential equations describing mass and charge transport in the solid (electrode particles) and liquid (electrolyte) phases. An extension of this is the homogenized pseudo-2D model, where all electrode particles are assumed to be identical spheres. This monodisperse simplification neglects the polydispersed, non-spherical morphologies that characterize real electrodes. Such heterogeneities often cause non-uniform current distribution and affect performance and lifetime. While spherical approximations may be acceptable for some cathodes (e.g., NMC), graphite anodes cannot be accurately represented in this way. Graphite particles are flake-shaped, with one dimension much smaller than the others, as shown in FESEM (Field Emission Scanning Electron Microscopy) images from Fig. 1b and Fig. 1c. Hence, the spherical assumption is far from reality. Recent work by Lu et al. [2] also demonstrated that

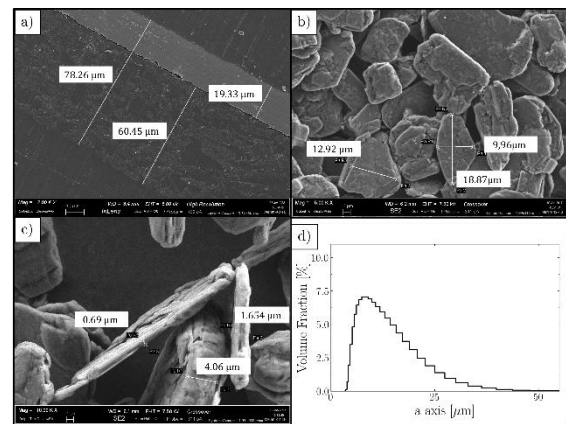


Figure 1. (a) FESEM image of electrode of half cell: graphite and separator. (b) FESEM image of graphite layer. (c) FESEM image of graphite particle. (d) PSD of graphite particles within electrode.

proper in-silico electrode geometry significantly influences intra-particle lithiation predictions. Motivated by these challenges, we developed an automatic Java script to generate pore-scale, three-dimensional transient computational models (4D models) of LiB half-cells. The script interfaces with the COMSOL Multiphysics 6.3 API and collects all input parameters in text files, including particle geometrical characterization and physico-chemical properties. This enables flexible and automated

dataset creation, allowing systematic variation of both physical and geometric properties. In particular, it facilitates the study of different active material types, both anodic and cathodic, with varying particle size distributions, equilibrium potentials, and diffusion coefficients.

Using this tool, we created three electrode geometries of increasing complexity: monodisperse spheres, polydisperse spheres, and polydisperse ellipsoids. The ellipsoidal case was chosen to better approximate graphite morphology, offering tunable aspect ratios to mimic flake-like particles. We compared intercalated lithium concentrations, and discharge curves with experiments, demonstrating the importance of realistic geometry and the flexibility of our workflow [3].

Model Set Up

In this section, we illustrate the main steps used for geometry generation. The electrode geometry is considered static during the discharge process, since thermal–mechanical effects, which could alter the electrode morphology especially under fast cycling conditions, are not taken into account.

Electrodes were recreated using Discrete Element Method (DEM) [4] simulations combined with the periodic compression routine implemented in the open-source code **Yade** (version 2022.01a), coupled with **Blender** (version 4.3.2). These software packages were chosen because both provide Python APIs (version 3.10.4), allowing the automatic generation of different geometries in a straightforward way. This coupling also makes it possible to produce particles with complex geometries relatively quickly.

The workflow begins with the definition of two key inputs: the particle size distribution (PSD) and the aspect ratio (AR) between the two largest semi-axes. The PSD is used to generate polydisperse packings, while the AR allows the transformation of spherical particles into ellipsoids. Field Emission Scanning Electron Microscopy (FESEM) images of graphite electrodes were analyzed to determine characteristic particle dimensions. Graphite particles are typically flake-shaped, with one dimension much smaller than the other two. Therefore, they were modeled as flattened ellipsoids with semi-axes a , b , and c , where $a > b \gg c$. The thickness ($2c$) was fixed at $3 \mu\text{m}$, based on the average value obtained from experimental measurements. The major axis was derived from the experimental PSD (See Fig. 1d), while the minor axis was calculated from the aspect ratio measured from FESEM images, as shown in Fig 1c.

Once the input data were collected, DEM simulations were carried out in Yade to generate an

initial box of spheres, each with a radius equal to the major axis of the corresponding ellipsoid. This step ensures that particle–particle interpenetration is avoided during the transformation into ellipsoids. Yade provides the position and radius of each particle, which are then passed to Blender, where each sphere is replaced with an ellipsoid inscribed within it, oriented to mimic the effect of the calendaring process, where particles tend to align parallel to the current collector. A second DEM simulation in Blender further compacts the electrode structure by finalizing particle sedimentation.

The result is a detailed description of each particle with nine degrees of freedom: position of the center (x , y , z), three dimensions (a , b , c), and rotation around the three axes. These geometrical parameters are used as input for COMSOL Multiphysics 6.3, along with the physical parameters such as equilibrium potential, diffusion coefficient, and electrical conductivity, that may be function of the State of Charge (SoC).

To facilitate meshing, particles were slightly enlarged (by 1%) in each dimension to improve contact points between neighboring particles. Any fragment outside the central electrode block or not connected to the main structure were automatically removed, to avoid numerical mismatches. After adding the separator, all domains and surfaces were labeled and assigned their respective materials and physics. The system was then meshed with 180,000 to 300,000 elements, with an element mesh size between $h_{min}=0.85 \mu\text{m}$ and $h_{max}=6.6 \mu\text{m}$, to have a good compromise between computational cost and accuracy.

As mentioned earlier, we adopted the script to generate three electrode morphologies of increasing complexity: (i) monodisperse spheres, (ii) polydisperse spheres, and (iii) polydisperse ellipsoids, the latter being the most realistic representation of graphite particles. Each electrode was modeled with a thickness of $60 \mu\text{m}$ and a separator of $20 \mu\text{m}$ (see Fig 1a), with a lateral width of $20 \mu\text{m}$ in both X and Y directions. Discharge simulations at different current rates (C-rates) were then performed, and the intercalated lithium concentration within the active particles, as well as the discharge curves, were analysed and compared.

Governing Equations

The electrochemical model solved in this work describes the conservation of charge and mass in both the solid active material and the electrolyte of a lithium-ion battery [5]. To do so, we coupled Battery Design Module (BDM) and Chemical Species Transport (CST) from COMSOL Multiphysics.

The system is simplified by neglecting degradation phenomena such as the Solid Electrolyte Interphase (SEI) formation and growth, in order to isolate the fundamental mechanisms of lithium transport and

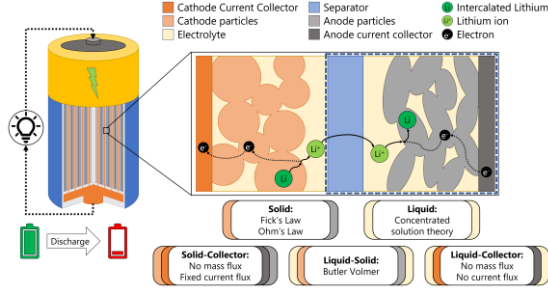


Figure 2. Schematic representation of the LiB cell during a discharge process with the most relevant equations. The blue dashed line highlights the half-cell simulated in this work.

intercalation. The main PDEs solved in this model are highlighted in Fig. 2.

The state of charge (SoC) is defined as the average concentration of intercalated lithium normalized between its values at 0% and 100% SoC:

$$SoC = \frac{\frac{1}{V^s} \int_{V^s} c^s dV^s - c_{0\%}^s}{c_{100\%}^s - c_{0\%}^s}$$

where c^s is the intercalated Li concentration, V^s is the active material volume, and $c_{100\%}^s - c_{0\%}^s$ is the concentration difference between the fully lithiated and fully delithiated states. This definition ensures that SoC varies between 0 and 1. The applied current is related to the C-rate, which specifies the reciprocal of the time required to complete a discharge. The total current is calculated as:

$$i = c_{max}^s ((SoC)_{max}^s - (SoC)_{min}^s) F V^s C_{rate}$$

where c_{max}^s is the maximum intercalated lithium concentration, F is the Faraday constant, and C_{rate} is the inverse of time required to fully charge or discharge the battery. Charge conservation in the solid phase is described by Ohm's law:

$$\nabla \cdot (\mathbf{K}^s \nabla \phi^s) = 0$$

where \mathbf{K}^s is the solid-phase electrical conductivity and ϕ^s is the electric potential. In parallel, the transport of lithium within the solid particles is governed by Fick's law of diffusion:

$$\frac{\partial c^s}{\partial t} = \nabla \cdot (\mathbf{D}^s \nabla c^s)$$

where \mathbf{D}^s is the diffusion coefficient in the solid phase and c^s is the intercalated Li concentration.

On the other hand, the transport equations related to the charge and mass conservation of lithium ions in the electrolyte are solved by applying concentrated solution theory:

$$\frac{\partial c^\ell}{\partial t} = \nabla \cdot \left[\left(\mathbf{D}^\ell - \frac{2RT}{F^2} (1 - t^+) t^+ \mathbf{K}^\ell \frac{1}{c^\ell} \right) \nabla c^\ell + \frac{t^+}{F} \mathbf{K}^\ell \nabla \phi^\ell \right]$$

$$0 = \nabla \cdot \left[\left(-\frac{2RT}{F} (1 - t^+) \mathbf{K}^\ell \frac{1}{c^\ell} \right) \nabla c^\ell + \mathbf{K}^\ell \nabla \phi^\ell \right]$$

where c^ℓ is the lithium-ion concentration in the electrolyte and ϕ^ℓ is the electrolyte potential, \mathbf{D}^ℓ and \mathbf{K}^ℓ are the diffusion and the electric conductivity coefficients respectively, R is the gas constant, and T is the temperature. In the lithium foil, we evaluated the total current \vec{N} and mass \vec{J} flux as follows:

$$\vec{N} = \pm \frac{i}{A_{cc}}; \quad \vec{J} = \pm \frac{i}{F A_{cc}}$$

where A_{cc} is the area of the lithium foil, and i is the current calculated above.

The flux sign is positive for discharge (lithium diffuses from the foil to the electrode) and negative for charge (lithium diffuses from the electrode to the lithium foil).

On the current collector side, we distinguish two possible situations: the electrolyte-current collector interface and the electrode-current collector interface. The mass flux is null in both cases, instead, the current flux is different from zero only at the electrode-current collector interface in which it is equal and opposite in sign to \vec{J} .

The last boundary condition applied in the model is the mass and charge transfer at the liquid-solid interface. Notably, electrochemical charge-transfer reactions cause the continuum exchange between liquid and solid phases of Li ions, intercalated Li, and electrons following the reaction mechanism illustrated in Fig. 2. The current density developed from an electrochemical reaction at the liquid-solid interface is called faradic current density and can be expressed through the well-known Butler-Volmer formalism:

$$i_{BV} = i_0 \left[\exp\left(\frac{\alpha_a F \eta}{RT}\right) - \exp\left(-\frac{\alpha_c F \eta}{RT}\right) \right]$$

where i_0 is the reference current density, α_a and α_c are the anodic and cathodic symmetry factors and here we assume $\alpha_a = \alpha_c = 0.5$. The last term that appears in the Butler-Volmer equation is the over-potential $\eta = \phi^s - \phi^\ell - E_{eq}^s$, meaning that in the

reversible reaction $Li_s \leftrightarrow Li_s^v + Li_l^+ + e_s^-$ less energy is recovered than thermodynamics predict.

Simulation Results and Discussion

In this work, three model electrode systems were generated and compared: monodisperse spheres, polydisperse spheres, polydisperse ellipsoids.

For each configuration, discharge curves and the concentration of intercalated lithium within the particles were analysed. Furthermore, the effect of different operational conditions was explored by simulating four different discharge rates: C/10, C/5, C/3, and 1C. This allowed us to systematically assess how morphology influences performance across a range of applied currents.

In order to validate the model, we compared the simulated discharge curves with experimental data obtained in our laboratory. The experiments were carried out on coin cells assembled with commercial graphite electrodes. Experimental discharges were performed at a current value corresponding to C/10, which completes a full discharge in 10 hours. Consequently, model validation is restricted to simulations performed at the same rate. This approach is necessary because higher C-rates are affected by polarization phenomena and cause degradation effects, which are not explicitly considered in the present study. The main operating conditions and geometrical parameters of the modeled electrodes are summarized in Tab 1. Physical coefficients for the electrolyte phase were treated as average values, since they vary with the lithium-ion concentration.

| Parameter | Value |
|-------------|---|
| c_0^s | 0 [mol/m ³] |
| c_0^l | 1000 [mol/m ³] |
| c_{max}^s | 31507 [mol/m ³] |
| SoC_{max} | 0.95 |
| SoC_{min} | 0 |
| K^s | 100 [S/m] |
| K^l | 0.743 [S/m] |
| D^s | 1.317×10^{-14} [m ² /s] |
| D^l | 3.613×10^{-10} [m ² /s] |
| α_a | 0.5 |
| α_c | 0.5 |
| t^+ | 0.363 |
| h_{min} | 0.85×10^{-6} [m] |
| h_{max} | 6.6×10^{-6} [m] |
| Δx | 20×10^{-6} [m] |
| Δy | 20×10^{-6} [m] |
| Δz | 60×10^{-6} [m] |
| sep | 20×10^{-6} [m] |

Table 1. Parameters used in the 4D resolved electrochemical model.

The full concentration-dependent data are available within the simulation script.

To assess the accuracy of the digital replicas, we first compared porosity values. Experimental porosity was measured from FESEM images of three independent electrode samples and showed a value of about 0.3 with uncertainty of approximately 10%. Digital porosity values were extracted from the three computational geometries, evaluating the volume ratio in COMSOL. The results, reported in Tab. 2, indicate that both the polydisperse spheres and ellipsoids fall within the experimental range, while the monodisperse sphere configuration deviates significantly.

| Geometry | Porosity | Specific Surface [m ² /cm ³] | Tortuosity |
|----------------------|----------|---|------------|
| Monodisp. Spheres | 0.376 | 9.29 | 2.05 |
| Polydisp. Spheres | 0.271 | 9.90 | 7.8 |
| Polydisp. Ellipsoids | 0.301 | 5.23 | 2.33 |

Table 2. Geometrical descriptors of the three types of reconstructed electrodes, compared with the experimental value.

This already suggests that monodisperse spherical packings cannot faithfully represent real graphite electrodes. Despite the scatter in experimental porosity measurements, both polydisperse spheres and ellipsoids provide geometrically consistent models. In addition to porosity, two other descriptors were evaluated computationally: the specific surface area and tortuosity. Specific surface was defined as the solid-liquid interface area normalized by the electrode volume. Tortuosity was calculated in the separator-current collector direction using the TauFactor algorithm in MATLAB. Experimental comparison for these values is more difficult. Commercial graphite powders typically report specific surface areas that include contributions from internal channels, which are not directly represented in the COMSOL-based digital electrode. As a result, the computational values obtained are systematically lower. However, these descriptors remain valuable for comparing trends across the simulated systems. Notably, the ellipsoidal configuration exhibits significantly higher tortuosity and specific surface than both spherical cases.

The next step is to analyze the electrochemical response. To begin, discharge curves at C/10 were compared against the experimental benchmark. In the figures, the continuous red line corresponds to ellipsoidal particles, the blue dash-dot line to polydisperse spheres, the green dashed line to monodisperse spheres, and the black dotted line to

the experimental curve. A double-logarithmic representation was used to highlight the distinct

stages of graphite lithiation, which are not as clearly visible in linear plots.

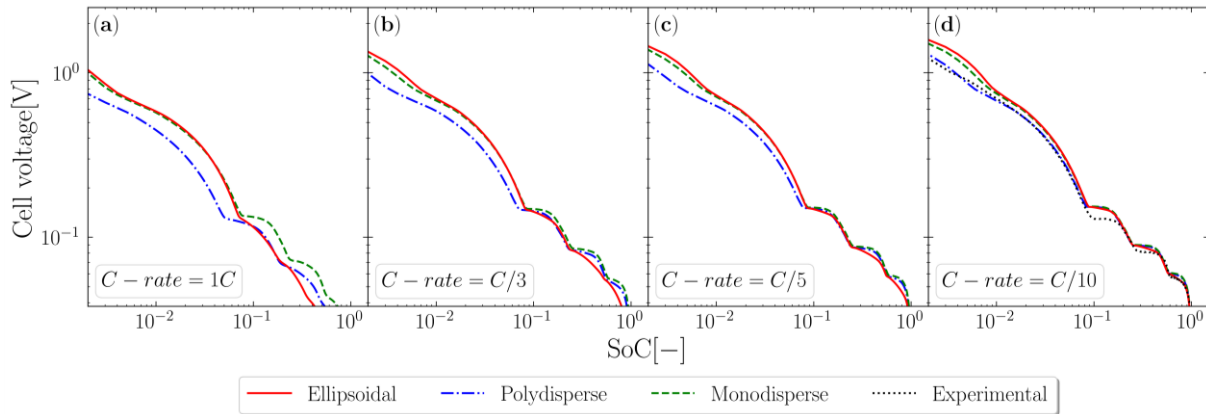


Figure 3. Discharge curves as a function of the SoC. The continuous red line represents the system with ellipsoidal particles, the blue dashed dot line refers to the electrode with polydisperse spheres, the green dashed line to the system formed by monodisperse spheres, and the black dotted line to the experimental data.

The comparison at $C/10$ from Fig. 3d shows that all three computational systems reproduce the experimental discharge curve reasonably well. This has two implications. First, it provides a second confirmation, after porosity, that the generated digital electrodes capture essential features of the real system. Second, it suggests that electrode morphology has a limited impact on discharge behavior under low current conditions. At $C/10$, lithium-ion transport within the electrolyte is sufficiently slow that gradients do not develop significantly, regardless of particle shape.

When the discharge rate is increased, however, the impact of morphology becomes evident. At $C/5$ and $C/3$, the curves begin to diverge. The electrode with ellipsoidal particles deviates most noticeably from the spherical models, particularly at graphite stage transitions where the slope of the discharge curve changes sharply. At $C/3$, both the polydisperse and monodisperse sphere systems underpredict the potential drop, highlighting their inability to capture transport limitations. At even higher rates, such as $1C$, the differences are striking. The spherical systems exhibit delayed or muted voltage responses compared to the ellipsoidal system, which more realistically reflects experimental trends reported in the literature. A deeper understanding of these differences can be obtained by analysing local concentration fields within the electrodes. Contour plots of the intercalated lithium concentration from Fig. 4 were extracted at half discharge ($\text{SoC}=50\%$) for all systems and rates.

At low current value, with C -rate equal $C/10$, the contour plot confirms the results of the discharge curves: vertical concentration gradients along the separator-collector direction are negligible across all systems because electrode morphology has a limited impact on discharge behavior under low current

conditions. The ellipsoidal system, however, already shows slightly higher concentrations near the separator, indicating the occurrence of transport heterogeneity.

Going up to $C/5$, the ellipsoidal electrode exhibits a marked vertical gradient, with higher lithium concentrations near the separator. The polydisperse sphere system shows both enhanced radial but small vertical gradients, while the monodisperse system continues to present a nearly uniform concentration gradient.

At $C/3$, the vertical gradient in the ellipsoidal system becomes strong, but radial gradients remain small, suggesting that the elongated particle shapes primarily affect transport through the electrode thickness. In contrast, the polydisperse sphere system exhibits both vertical and radial gradients. The monodisperse system again shows minor change, reinforcing that its oversimplified structure suppresses realistic transport phenomena.

Finally, when the current value is high, with C -rate equal to $1C$, even the monodisperse system begins to exhibit vertical gradients. In the polydisperse system, both radial and vertical gradients become marked. The ellipsoidal system shows the strongest heterogeneity, with lithium concentrations varying dramatically along the separator-collector direction and exhibiting a clear advancing concentration front. These trends directly correlate with the tortuosity values reported earlier: the elongated ellipsoidal particles force lithium ions to follow longer, more convoluted paths, leading to larger macroscopic gradients.

The presence of strong vertical gradients has also been widely observed experimentally, for example by X-ray tomography and other advanced imaging techniques [6]. In ellipsoidal configurations, the elongated particles act as obstacles that reduce the

effective diffusivity of the electrolyte phase. This geometric constraint amplifies the separation between regions close to the separator and those closer to the current collector, directly influencing

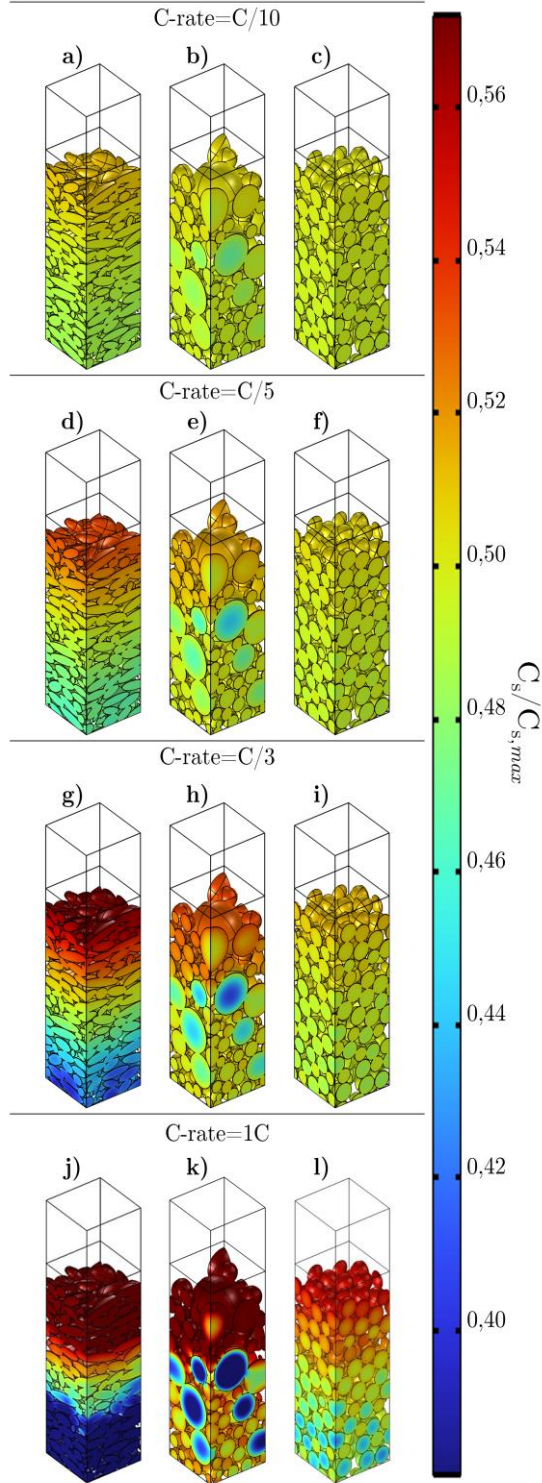


Figure 4. Local intercalated lithium concentration within the electrode. Images taken at half discharge, $SoC=50\%$. First row (a, b, c): $C\text{-rate}=C/10$; second row (d, e, f): $C\text{-rate}=C/5$; third row (g, h, i): $C\text{-rate}=C/3$; fourth row (j, k, l): $C\text{-rate}=1C$. First column (a, d, g, j): ellipsoidal particles; second column (b, e, h, k): polydisperse spherical particles; third column (c, f, i, l): monodisperse spherical particles.

discharge behavior. By contrast, spherical packings present lower tortuosity, which allows ions to move more freely, producing more homogeneous lithiation.

The key outcome of this analysis is that only models including polydisperse ellipsoidal particles reproduce the complex transport behavior observed experimentally. Simplified spherical models, whether mono- or polydisperse, fail to capture critical concentration gradients that strongly influence performance at practical discharge rates.

This has important implications. Local concentration profiles of lithium in the active material, in the electrolyte, and at their interface determine where and when degradation processes occur. Since all irreversible degradation phenomena, such as SEI formation, lithium plating, and mechanical fracturing, are strongly dependent on local conditions, accurate computational prediction requires realistic electrode geometries.

Our study therefore demonstrates the importance of including morphological complexity in 4D computational models of LiBs. By adopting ellipsoidal particles derived from real morphological data, we are able to replicate experimental behavior with greater fidelity. Future work will extend this approach to explicitly study degradation phenomena, with a particular focus on SEI formation, which is intimately linked to local lithium concentrations and gradients.

Conclusions

This study addresses the limitations of conventional LiB models by emphasizing the importance of accurate electrode geometrical representation. Traditional models often approximate graphite particles as spheres, but this assumption fails to capture the anisotropic geometry of real graphite, which significantly affects electrochemical behavior. Using electrochemical half-cell models, we demonstrate that a more realistic particle representation improves the understanding of intra-particle lithiation and provides more accurate predictions of battery performance.

To achieve this, we developed an automatic script in Python and Java which interfaces with the COMSOL API capable of replicating electrodes with varying physical and geometric properties. We adopted this script to generate and compare different electrode morphologies and configurations, highlighting the critical role of particle geometry in transport and

reaction dynamics. Accurate geometry influences particle arrangement, porosity, and specific surface area, which are crucial in electrochemical models governed by surface reactions. Inaccurate geometrical assumptions, such as the use of spherical particles, promote isotropic transport properties and uniform reaction rates, but fail to capture localized concentration gradients and reaction rate variations observed in real electrodes. By contrast, ellipsoidal or flake-like particles introduce anisotropy and high tortuosity, leading to more complex ion distributions and non-uniform electrochemical behavior. These differences underscore the necessity of accurate geometrical models for both accurate prediction and optimization of battery systems.

Our findings suggest that improved geometrical models can enhance the prediction of battery performance, inform better electrode design, and contribute to more efficient and longer-lasting LiBs. This approach not only refines theoretical understanding but also provides practical tools for advancing LiB technology in line with global energy sustainability goals.

Future research should address these limitations by incorporating the automatic script with more features, like realistic particle morphologies, degradation processes, and thermal dynamics. Exploring these aspects with oversimplified geometries would not provide meaningful insights and could hinder progress in battery design.

Furthermore, being able to produce automatically and in a short time complex, detailed, and realistic 4D models offers a huge help in both design experiments and dataset creation. By combining accurate morphology with electrochemical and thermal effects, future simulations will enable more comprehensive and predictive modeling of LiBs. Such detailed in-silico representations are essential for capturing the complex interplay of phenomena within batteries and for guiding the development of safer, more reliable, and more efficient energy storage systems.

References

- [1] M. Doyle, T. Fuller and J. Newman, "Modeling of Galvanostatic Charge and Discharge of the Lithium/Polymer/Insertion Cell.," *Journal of The Electrochemical Society*, vol. 140, no. 6, p. 1526, 1993.
- [2] X. Lu, M. Lagnoni, A. Bertei, S. Das, R. Owen, Q. Li, K. O'Regan, A. Wade, D. Finegan, E. Kendrick, M. Bazant, D. Brett and P. Shearing, "Multiscale dynamics of charging and plating in graphite electrodes coupling operando microscopy and phase-field modelling," *Nature Communications*, vol. 14, no. 1, p. 5127, 2023.
- [3] A. Lombardo Pontillo, A. Marcato, D. Versaci, D. Marchisio and G. Boccardo, "Comparative Analysis via CFD Simulation on the Impact of Graphite Anode Morphologies on the Discharge of a Lithium-Ion Battery.," *Batteries*, vol. 11, no. 7, p. 252, 2025.
- [4] G. Boccardo, F. Augier, Y. Haroun, D. Ferré and D. Marchisio, "Validation of a novel open-source work-flow for the simulation of packed-bed reactors," *Chemical Engineering Journal*, vol. 279, pp. 809-820, 2015.
- [5] G. M. Goldin, A. M. Colclasure, A. H. Wiedemann and R. J. Kee, "Three-dimensional particle-resolved models of Li-ion batteries to assist the evaluation of empirical parameters in one-dimensional models," *Electrochimica Acta*, vol. 64, pp. 118-129, 2012.
- [6] K. Yao, J. Okasinski, K. Kalaga, I. Shkrob and D. Abraham, "Quantifying lithium concentration gradients in the graphite electrode of Li-ion cells using operando energy dispersive X-ray diffraction," *Energy Environ. Sci.*, vol. 12, no. 2, pp. 656-665, 2012.

Acknowledgements

This research was funded by the large-scale European research initiative Battery 2030+ (under grant agreement No. 957213) and the Battery Interface Genome – Materials Acceleration Platform project (www.big-map.eu, under grant agreement No. 957189).

This work was funded by the European Commission within the Horizon Europe research and innovation program (BatCat, under grant agreement No. 101137725).

The authors also acknowledge the financial support from ICSC (Centro Nazionale di Ricerca in High Performance Computing, Big Data and Quantum Computing, funded by the European Union–NextGenerationEU).